International Journal of Current Engineering and Technology
E-ISSN 2277 – 4106, P-ISSN 2347 – 5161

Available at http://inpressco.com/category/ijcet

Research Article

Ground Penetrating Radar Technique for Assessing Pavement Thicknesses and Bridge Deterioration

Hussein H. Karim#*, Hasan H. Joni# and Aram A. Dawood#

#Building and Construction Engineering Department, University of Technology, Baghdad, Iraq

Accepted 25 Sept 2016, Available online 04 Oct 2016, **Vol.6, No.5 (Oct 2016)**

Abstract

Ground penetrating radar (GPR) has gained increasing popularity in quality control surveys of new and existing road, highways and other structures in the field of pavement engineering due to its greatest advantages as non destructive testing in comparison to the traditional drill core or other methods as well as costs are low and surveys can be performed quickly and data collection can be 2D or 3D displayed. GPR surveys using different types of antennas (250, 500, 800, and 1000 MHz) were carried out along many traverses at different sites. From the intensive implementation of this technique for pavement engineering investigations, data filtering and post processing give results showed pavement layers thickness estimation, damage detection and diagnosis, inspection and monitoring damaged post-tension bridge deck and piers. Several softwares were used for information extraction, processing and 2D or 3D displaying. 3-D imaging radargrams obtained by special softwares reflect better displays over the deteriorated 2-D sections. However, 2-D imaging radargrams gained by 1 GHz offer massive date collection on a bridge deck can be used to distinguish concrete damaged areas or corroded and deflected reinforcement, besides the reinforcement orientations of the doubly reinforced deck were clearly visible. The migration technique was utilized for reinforcement spacing in bridge pier and deck to restore the real location and shape of the reflecting bar.

Keywords: *GPR, HMA, Debonding, Pavement thickness, Post-tension bridge, Amplitude reflection coefficient, Migration technique.*

Introduction

Usually, the pavement will itself consist of several individual layers of slightly different types of material, to provide good load-spreading ability, and give a smooth ride for vehicles. However, the specific in-situ conditions of a bituminous material lead to variations in properties between materials that are nominally the same. Debonding of layers, stripping, material deterioration, aging, variation in local aggregate used, moisture amounts can all lead to variations in the material engineering properties. Typically, modern pavements have design lives of 20 or 30 years before any major maintenance or reconstruction is required, but pavement structures will deteriorate over time before this design life is reached. Deterioration can be caused by a number of factors, the main ones being the number and magnitude of vehicle loadings to which the pavement is subjected. To maximize the functional life of a pavement, it is essential to obtain information about the in-service condition, so that any deterioration can be identified or anticipated and maintenance treatments can be planned.

***Corresponding author Dr. Hussein H. Karim** is working as Professor; **Dr. Hasan H. Joni** as Assistant Professor and **Aram A. Dawood** is M.Sc. in Highway and Transportation Engineering

As conventional methods of pavement failure investigation are destructive testing which include extraction and examination of core samples from rutted sections, expensive required a lot of work and time to be performed, so the need to geophysical methods have been increased as they are nondestructive, time and cost-effective tools to provide information about the pavement structures (Muller, 2001; Amer *et al*., 2014).

Ground penetrating radar (GPR) is one of the common geophysical technique has been used for assessing pavement layer thickness and bridge deck condition, measurement of depth of rebar, and dowel location (Barnes *et al*., 2004; Al-Qadi *et al*., 2005).

The GPR method provides a high resolution image of subsurface features in the form of a cross section view that is essentially a map of the variation in ground electrical properties. These can be correlated with physical changes such the soil bedrock interface, the boundaries between asphaltic layers, water table, underground structures such as pipes, cables and tunnels as well as voids and cavities. The antennas physical size or dimension limits the frequency (or wavelength) of the transmitted pulse. A high frequency waveform (short wavelength) will provide more detailed or higher resolution image than a low

frequency wave form, but the higher frequencies are attenuated or absorbed at a greater rate (Griffin and Pippett, 2002).

This article presents the results of the integration of conventional investigation by core samples with GPR to generate detailed pavement condition information for flexible and composite pavements sections of the studied sites and to show the capability of GPR for inspection and monitoring damaged post tension bridge.

Radio Waves Propagation

The electromagnetic wave propagates in air with the speed of light but in the ground the velocity of electromagnetic waves is reduced since it is dependent on the relative dielectric permittivity, the relative magnetic permeability, and the electrical conductivity (Charlton, 2008).

The velocity of electromagnetic waves in a host material is given by:

$$V_m = c/\sqrt{\left\{\left(\frac{\varepsilon_r \mu_r}{2}\right)\right\}[(1+P^2)+1]} \quad (1)$$

Where c is the velocity of light in vacuum c = 299,792,458 m/sec, P is the loss factor, and equals to ($\sigma/\omega\varepsilon_r$), σ is the electrical conductivity for materials in (mS/m), ω =2πf, f is the frequency (Hz), and ε_r is the relative dielectric permittivity. In addition, the radar signal velocity in low-loss materials (P≈ 0) which are responsive to radar sounding is related to ε_r (Davis and Annan, 1989).

Hence, the equation can be simplified to:

$$V_m = \frac{c}{\sqrt{\varepsilon_r}} \quad (2)$$

The amplitude and polarity of the wave reflected from a change in dielectric properties depends on the ratio of the two relative dielectric constants and is referred to as the reflection coefficient (Moore *et al*., 1980; Bhandarkar, 1993). The greater the difference between materials in the subsurface, the larger the amplitude of reflection generated, this can be quantified using the amplitude reflection coefficient (R*)* at the boundary:

$$R_{1,2} = \frac{\sqrt{(\varepsilon_r')_1} - \sqrt{(\varepsilon_r')_2}}{\sqrt{(\varepsilon_r')_1} + \sqrt{(\varepsilon_r')_2}} \quad (3)$$

As radio waves travel through the ground, there are a number of reasons in which the signal energy is reduced, therefore the reflection at a dielectric interface reduces the signal energy available for deeper reflection events (Reynolds, 1997). The attenuation factor is dependent on the electric conductivity (σ), magnetic (μ) and dielectric (ε) properties of the medium through which the signal is propagating through (Reynolds, 1997):

$$\alpha = \omega\left\{\left(\frac{\mu\varepsilon}{2}\right)\left[\left(1+\frac{\sigma^2}{\omega^2\varepsilon^2}\right)^{1/2} - 1\right]\right\}^{1/2} \quad (4)$$

The formulation is valid for non-magnetic materials only. In a low-loss medium, attenuation (dB/m) is most practically expressed by (Davis and Annan, 1989):

$$\alpha = \frac{(1.69\times10^3)\ \sigma}{\sqrt{\varepsilon_r}} \quad (5)$$

The degree of attenuation present in a material determines the achievable depth of penetration, along with other characteristics of the system. These characteristics are all interrelated and force a GPR operator to strike a balance between penetration depth and vertical resolution (Davis and Annan, 1989). Penetration depth in homogeneous media is mainly determined by wavelength λ.

$$\lambda = \frac{c}{f\sqrt{\varepsilon_r}} \quad (6)$$

The GPR illumination pattern is approximately elliptical in shape meaning that the footprint is always looking not only directly below the antenna but also in front, behind and to the sides (Davis and Annan, 1989), as it travels across the ground. In order to minimize interference from side readings, the long axis of the antenna should be aligned parallel to the direction of antenna movement (which is parallel to the electric field the antenna generates) (Conyers and Goodman, 1997).

$$A = \frac{\lambda}{4} + \frac{D}{\sqrt{\varepsilon_r+1}} \quad (7)$$

Where A is the approximate long dimension radius of footprint, B is approximate radius perpendicular to the long axis, λ is the center frequency wavelength of radar energy, and D is the depth from ground surface to reflection surface.

Field Exertion and Data Collection

The field work included different aspects extending from the structure condition speculations to the materialistic physical characteristics variations. It is concentrated on determining flexible and rigid pavement layer thicknesses and evaluation the condition of a bridge deck at different sites.

Currently, most of transportation agencies evaluate layer thickness and the properties of different pavement layers through the destructive process of extracting pavement cores. While, this procedure provides relatively accurate thickness measurements, it is time consuming, hazardous, requires traffic control, provides limited information (as cores are usually taken every 300 m), and cannot be performed annually since it adds to the pavement distress by causing man-made defects.

To define the accuracy of this technique for pavement thicknesses, two different antennas frequencies 500 and 800 MHz were used. For attaining appropriate horizontal resolution, short max. time window at different pulse rate intervals over 0.01, 0.03, and 0.05 m were chosen, since it has a significant effect on interface visualizing and picking distribution in determining pavement thicknesses. For such case study, two locations in Baghdad-Iraq were selected for both flexible and composite pavements sections, these are:

1. Palestine Street: Overlaid flexible pavement (N 33°20'56.38, E 44°26'20.73)
2. University of Technology: Composite pavement (N 33°18'43.38, E 44°26'55.66)

The radargrams of Profiles Nos. 587 and 558 using 800 and 500 MHz antennas, short max. time window, 0.01 m stacking are shown respectively for the overlaid flexible pavement (Figure 1a and b). While, Figure 2a and b represents the radargrams of Profiles Nos. 181 and 178, respectively for the composite pavement.

After achieving the survey, a correlation with radar data was performed by drilling two core samples with 10 cm diameter cutter shift for each study.

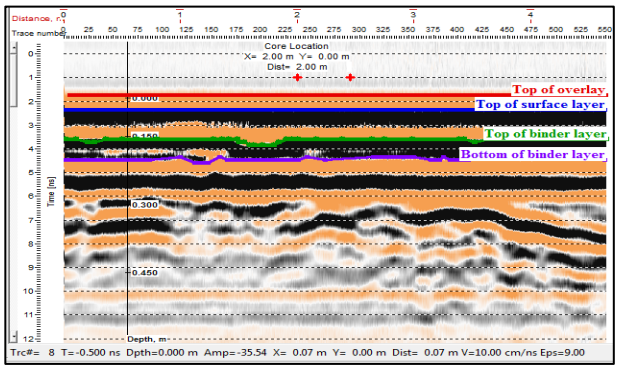

(a)

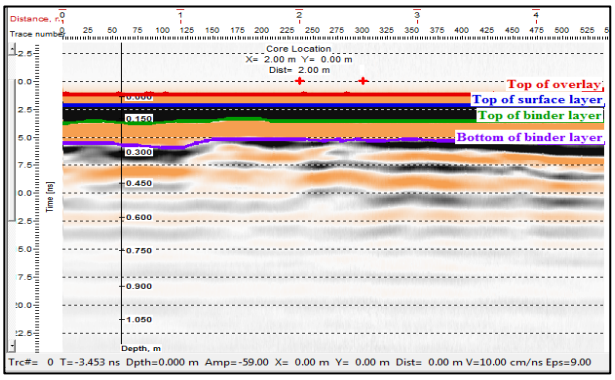

(b)

Figure 1: Radargrams for the overlaid asphalt pavement using short max. time window, 0.01 m trace stacking. (a) Profile No. 587 using 800 MHz antenna; (b) Profile No. 558 using 500 MHz antenna.

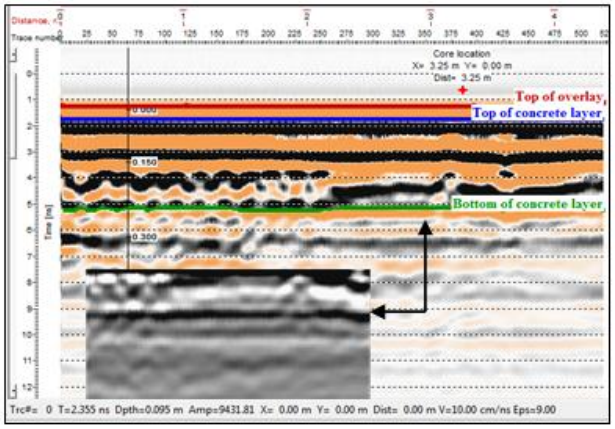

(a)

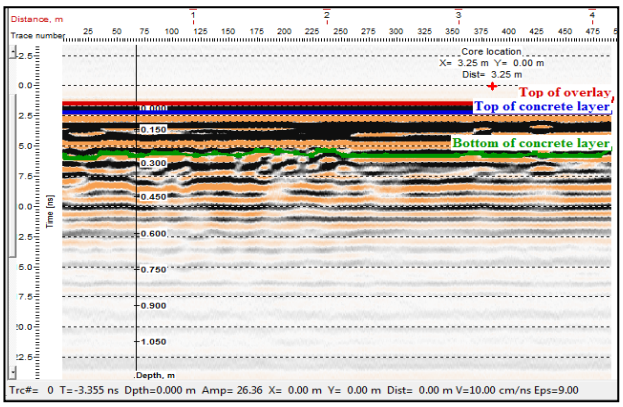

(b)

Figure 2: Radargrams for the composite pavement using short max. time window, 0.01 m trace stacking. (a) Profile No. 181 using 800 MHz antenna; (b) Profile No. 178 using 500 MHz antenna.

For a bridge deck condition assessment project, a post tension bridge in Daura-Yusufiyah province in Baghdad- Iraq had been inspected for extended defects on due to heavy impact explosion force effect beneath the expansion joint of the abutment. The bridge is of approximately 554 m in length, 14.3 m in width (including both of the sidewalks each of 1.65 meter), the deck is 0.90 m total depth, approximately 8.5 m and 6.20 m for top and lower pier flanks, respectively.

GPR applications on bridges usually concern a condition evaluation of a bridge deck. Therefore, significant applications have been studied on 63 surveyed profiles for both deck and pier including both two and three dimensional imaging.

Individual intentions for this study are clearly addressed for both bridge deck and pier column:

1) For Concrete Integrity

- Estimation of thicknesses for different structural layers of the bridge deck.
- Debonding, large cracks and caverns or any deteriorated areas within the structure.

- Moisture ingress at specific locations of the bridge deck.

2) For Reinforcement Condition

- The Orientation of reinforcement, including the longitudinal and stirrups spacing for the doubly reinforced deck.
- Concrete cover of reinforcement in both bridge deck and pier.
- Assessing rebar corrosion or damage.
- Position of post-tensioned tendons or its ducts.

GPR data are typically collected in direction perpendicular to the upper most rebar orientation. Thus, if the upper rebar orientation is transverse, then the data would be collected in the direction of traffic. As illustrated in Figure 3a and 3b sketched by using SketchUp Builder 2016, v.16.1.1450 software, seven GPR profiles were deployed along the bridge deck in lines parallel to the direction of traffic. The profile lines were perpendicular to the transverse direction of the upper most rebar. The field work procedures are presented in Figure 4.

The GPR scans of the bridge deck and pier column inspections were collected by MALA CU-II system with 1 GHz in cooperating with Ministry of Science and Technology. Site assessment was performed in a collaborative effort between Site defense Military Forces and the Ministry of Construction and Housing/S.C.R. B/Express way Directorate.

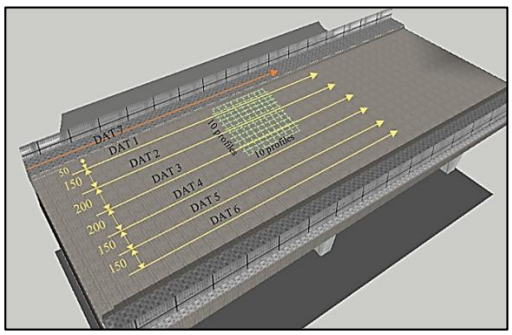

(a)

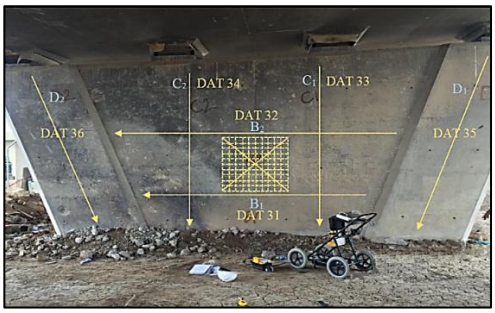

(b)

Figure 3: GPR profiles deployed on: (a) The bridge deck (b) The nearest pier from the deterioration. (Dimensions are in cm).

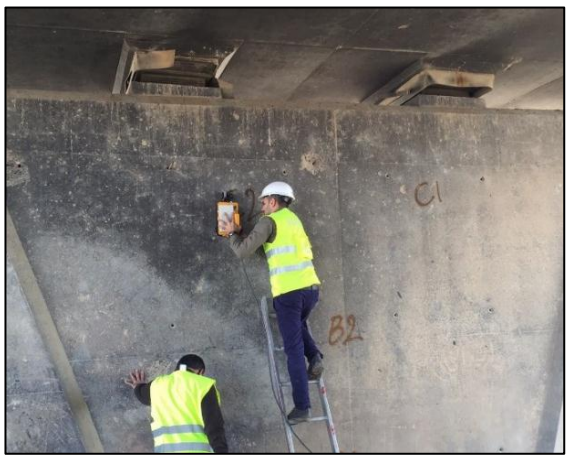

Figure 4: Field photos in Daura–Yusufiyah site, Baghdad-Iraq, during the bridge inspections.

Table 1: GPR thickness data simulation with core drilling using 500 and 800 MHz frequency

Layer	Point Interval (m)	Thickness (cm)			Absolute Deviation = |GPR – Core| (cm)		% Error in Measurements in Thickness of GPR	
		From GPR		From Core Drilling	500 MHz	800 MHz	500 MHz	800 MHz
		500 MHz	800 MHz					
Overlay	0.01	7.2	6.63	6.5	0.7	0.13	10.76	2
Surface		8.92	8.2	8.4	0.52	0.2	6.2	2.38
Binder		8.69	4.87	4.9	3.79	0.03	77.34	0.61
Total		24.81	19.7	19.8	5.01	0.1	25.30	0.50
Overlay	0.03	7.28	6.54	6.5	0.78	0.04	12	0.61
Surface		8.9	8.23	8.4	0.5	0.17	5.95	2.02
Binder		8.71	4.87	4.9	3.81	0.03	77.75	0.61
Total		24.89	19.64	19.8	5.09	0.24	25.70	0.80
Overlay	0.05	5.5	6.46	6.5	1	0.04	15.38	0.61
Surface		10.6	8.25	8.4	2.2	0.15	26.19	1.78
Binder		8.7	4.88	4.9	3.8	0.02	77.55	0.40
Total		24.8	19.59	19.8	5	0.21	25.25	1.06

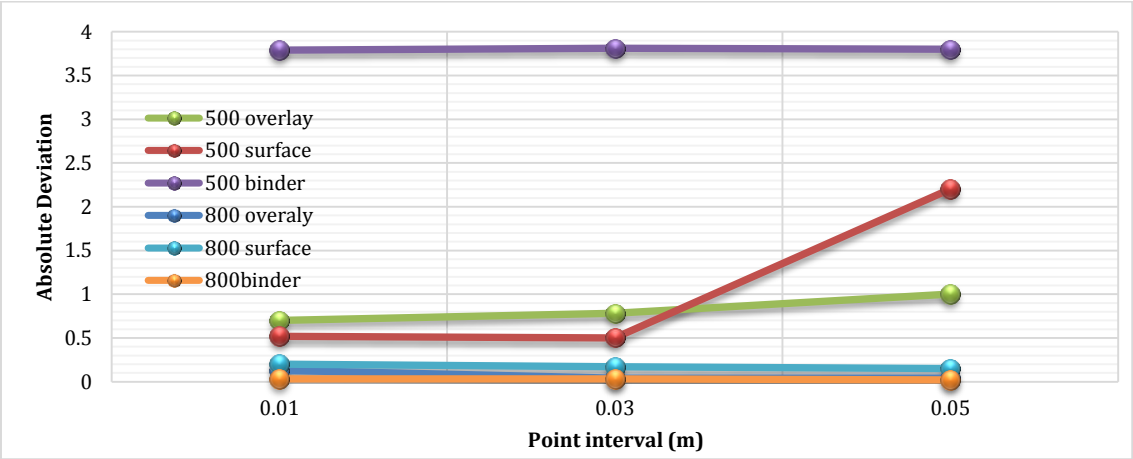

Figure 5: Effect of point interval variation and thickness deviations for different layers using 500 and 800 MHz antennas.

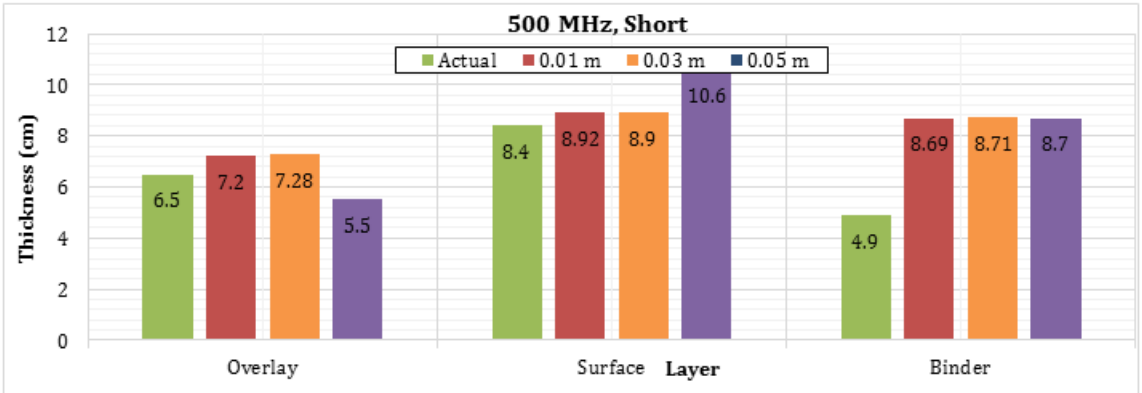

Figure 6: Thickness picking distribution for different layers and point intervals for 500 MHz antenna.

Results, Interpretation and Discussion

Accuracy of GPR for Estimating Pavement Layer Thicknesses

After picking the interfaces carefully and exported as full data tables, coring true data at certain points had also correlated with the radar data in order to give an accurate relation for the percentage error and deviations from the actual results for different point intervals.

For overlaid asphalt concrete pavement, Table 1 represents GPR thickness using 500 and 800 MHz

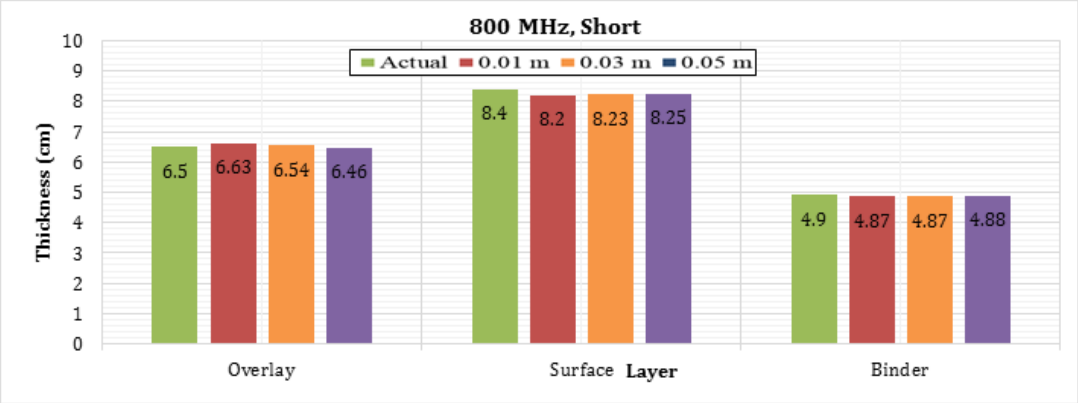

Figure 7: Thickness picking distribution for different layers and point intervals for 800 MHz antenna.

Table 2: GPR thickness data simulation with core drilling using 500 and 800 MHz frequency.

Layer	Point Interval (m)	Thickness (cm)			Absolute Deviation = |GPR – Core| (cm)		% Error in Measurements in Thickness of GPR	
		From GPR		From Core Drilling	500 MHz	800 MHz	500 MHz	800 MHz
		500 MHz	800 MHz					
Overlay	0.01	6.3	4.7	4.5	1.8	0.2	40	4.44
Concrete		20	19.4	19.8	0.2	0.4	1.01	2.02
Total		26.3	24.1	24.3	2	02	8.23	0.82
Overlay	0.03	6.3	4.7	4.5	1.8	0.2	40	4.44
Concrete		20	19.4	19.8	0.2	0.4	1.01	2.02
Total		26.3	24.1	24.3	2	0.2	8.23	0.80
Overlay	0.05	6.7	4.4	4.5	2.2	0.1	48.88	2.22
Concrete		19.9	19.5	19.8	0.1	0.3	0.50	1.51
Total		26.6	23.9	24.3	2.3	0.4	9.46	1.64

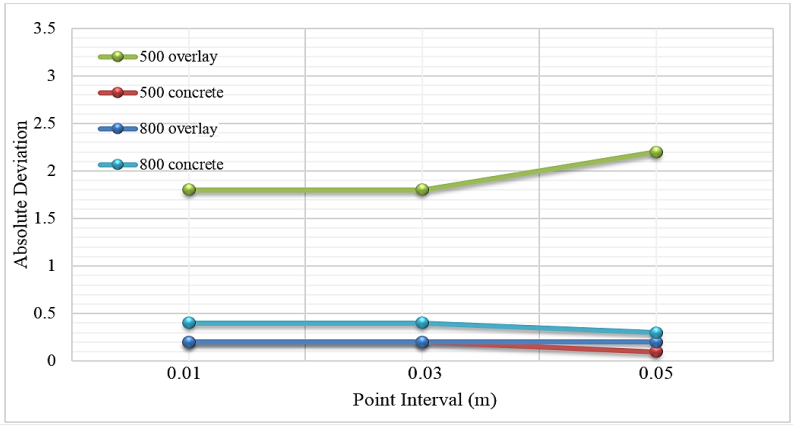

Figure 8: Effect of point interval variation and thickness deviations for composite pavement layers using 500 and 800 MHz antennas.

antennas and simulated with ground real date core drilling for the asphaltic overlay, surface and binder layers.

It is obvious that the trending shows higher deviations for the binder layer outputs ranging closely about 3.8 cm, which leads to percentage error about 77% along the 0.01, 0.03 and 0.05 m point interval. While, note that for both surface and overlay the percentage error significantly declines to about 6.2 and 10.7 respectively at 0.01 interval, also see Figure 5 and 6 for layers thickness distribution with different point intervals. From this behavior it can be concluded that the reflected pulse for interfaces near to pavement surface is identified more easily with lower deviations rather than the deeper interfaces visualized with 500 MHz frequency. But, a marked increase is noticed when performing the 0.05 m point interval for the surface layer. Besides, the percentage error for the overlay increases gradually at the three point intervals.

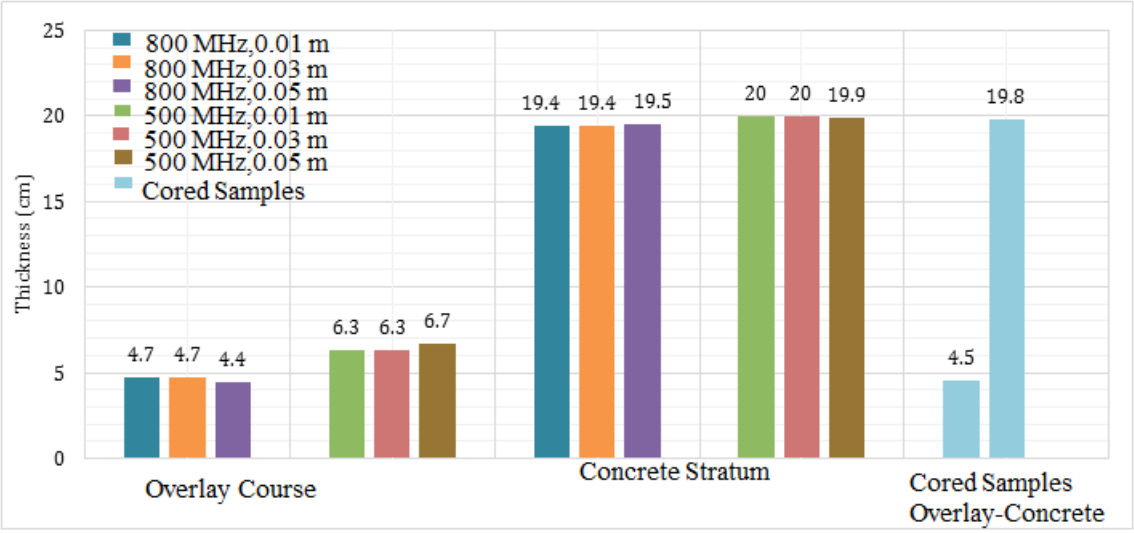

Figure 9: Thickness picking distribution for composite pavement layers and point intervals using 500 and 800 MHz antennas

However, a significant difference in deviation outputs were marked when the pavement layers inspected with the 800 MHz frequency, unstable trending for each layer is observed along the three intervals for each layer exported (Figures 5 and 7). As an overall, the maximum percentage error was about (1%) in total marked at 0.05 m interval, while the minimal percentage was (0.5%) in total thickness at 0.01 m point interval. As a result, it is truly sufficient to determine the flexible pavement thicknesses with 800 MHz frequency or higher with 0.01 m point interval that permit the analyst to determine the actual interfaces picking more clearly with minimal errors by increasing the number of traces collected per unite distance (i.e. increasing the horizontal resolution). These percentage errors can be varied depending on the data collection and the way that the analyst's process and interpret the outcomes.

For composite concrete pavement, the same previous procedures will be restated comprising the composite pavement to demonstrate the accuracy of this technique for both conditions. Table 2 represents GPR thickness data simulation with core drilling using 500 and 800 MHz frequency antennas respectively. The first table shows that the maximum deviations were noticed to range from 1.8 cm using the 0.01 and 0.03 m point interval for the asphaltic overlay, and about 2.2 cm is observed using the 0.05 m. While, minimum deviations were found for the concrete layer using the 0.01 and 0.03 m intervals, see Figures 8 and 9. Whereas, the total percentage error using 800 MHz were found to be approximately equal to 0.8% for 0.01 and 0.03 point intervals. Then, the total percentage error is increased to about 1.64% when the interval sets to 0.05 m.

The percentage errors presented from the composite pavements are typically less than for overlaid flexible pavements, since the interfaces are clearer to reflect, this may relate to layer materialistic variance (dielectric permittivity for asphalt concrete and rigid concrete mix).

Capability of GPR for Inspection and Monitoring Damaged Post Tension Bridge

The 1 GHz antenna has a depth of penetration of approximately 0.8 m in concrete, which is less than the full depth of deck structure but is well adequate to accurately locate the proximate layers of rebar and deck condition within the penetrated depth. In addition to visual inspections, traditional hammer sounding method has been also used to detect defects by striking the concrete surface along the studied profiles and surroundings, and listening to the responses, but this method was ineffective and did not promise for any condition conception of the slab during the study.

For this study, two softwares were used; the RadExplorer (v.1.4.2) software for 2D lines and the rest 20 individual files for deck were combined into a solid model to produce the 3D imaging using the Easy 3D (v.1.2.1) software. Processing steps involved in creating an exploration map of the structure under study. The first processing step implemented in a semi-automated manner, performs time zero correction, migration, and rebar reflection mapping. The next step is interactive interpretation and correlation.

The three-dimensional survey was processed using MALA Easy 3D software program with the corresponding Bridge Assessment Module. The results were used to produce a color coded deterioration map of the bridge deck under the area served of the grid with different depth layers (deterioration map) as illustrated in Figure 10. However, this represents only the conditions at the time of measurement. Changes in test conditions over time can influence the readings.

For cover survey, two methods were found to be necessitated in programming to perform the required behavior of the picked reinforcement reflections with

minimal error percentages either by manually picking reflection points or the short-time consuming through reflection picking method. In the first method, each pick must be fixed at the uppermost of the produced hyperbola. The reflection picking method with assistance of the migration technique was found to be useful for integrated objects, continuous layered interface and uniform voltage amplitude textures. Figure 11 represents an example for Profile No.4 by means of autofill method. Figure 12 displays the cover survey conducted on concrete bridge deck using reflection method picking after applying migration for DAT 1 and DAT 2. The cover picks in the first profile were ranged from about 2.75 to 5 cm and the cover varies densely by about 3.5 cm, while the second profile has similar trend ranging from 2.5 to 4.5 cm and highly distributed at approximately 3.75 cm.

Considering the three dimensional mesh grids, an arbitrary profile is selected for the longitudinal or major reinforcement (Figure 13). It is obviously noticeable that the upper slab comprises of double-layered reinforcement for the longitudinal direction, while the data after picking are exported and demonstrated that the upper longitudinal bars were at spacing of 13 to 18 cm, with some distorted locations. The lower longitudinal bars were distributed at intended spacing of 30 cm to be rendering from 27 to 34 cm.

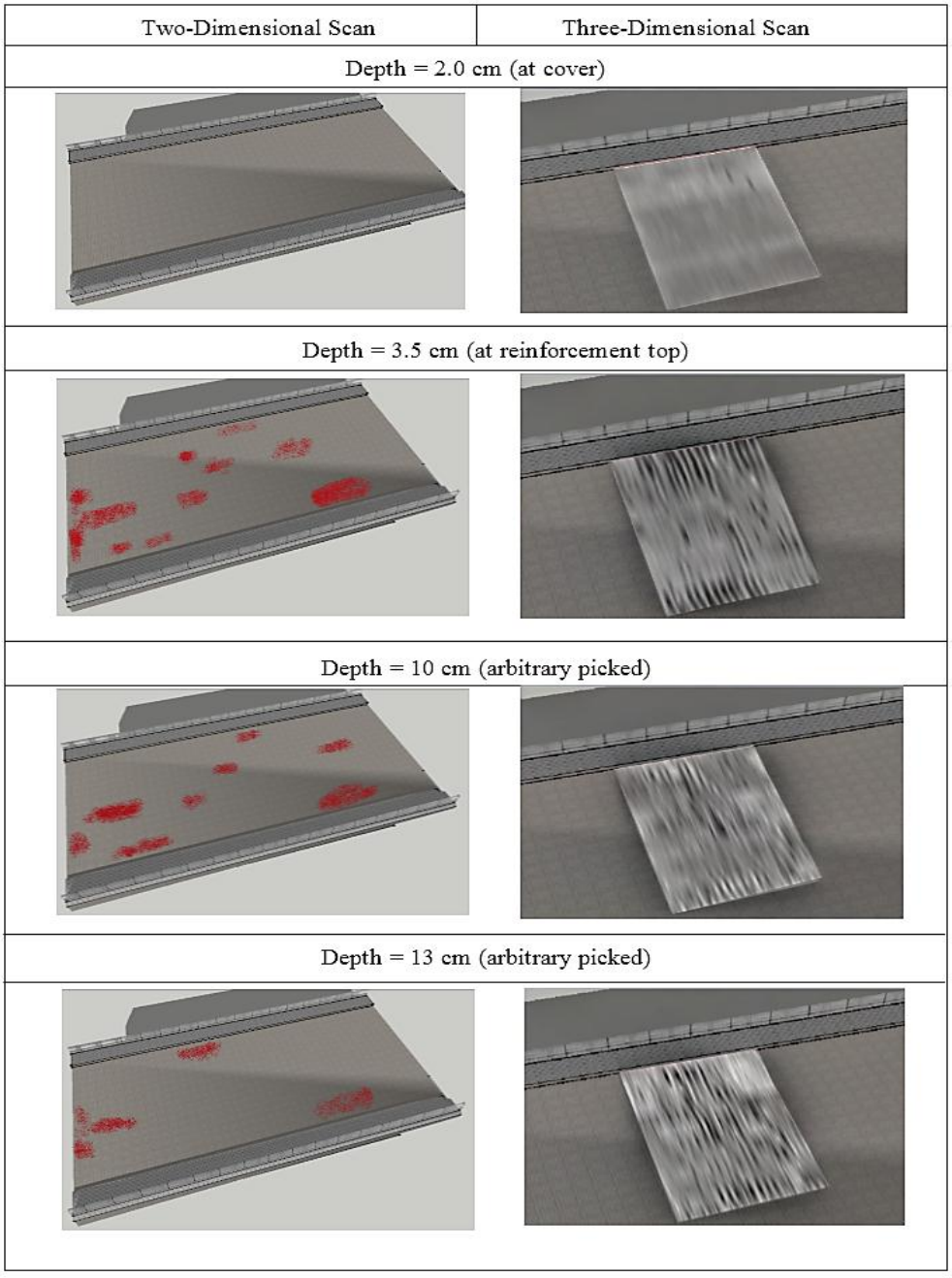

Figure 10: Vertical sliced processed data of possible moisture ingress (right) and possible defects along the first 20 meter at different depths (left).

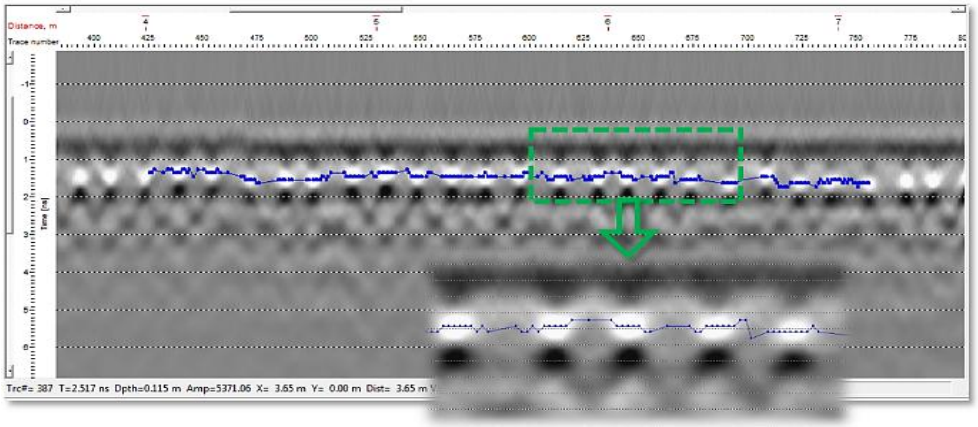

Figure 11: Reinforcement picking of radargram using autofill through picking mode after application the migration technique.

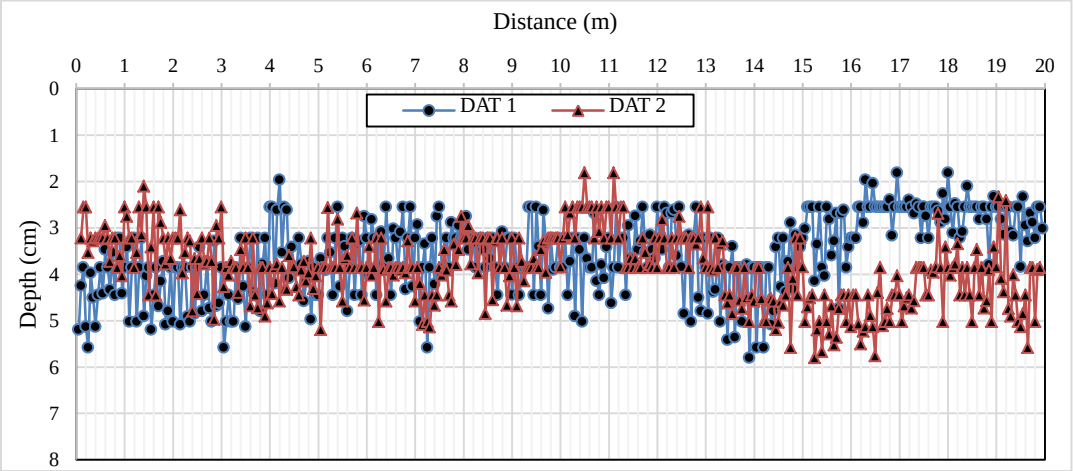

Figure 12: Cover survey conducted on concrete bridge deck using through picking method after application of migration for DAT 1 and DAT 2.

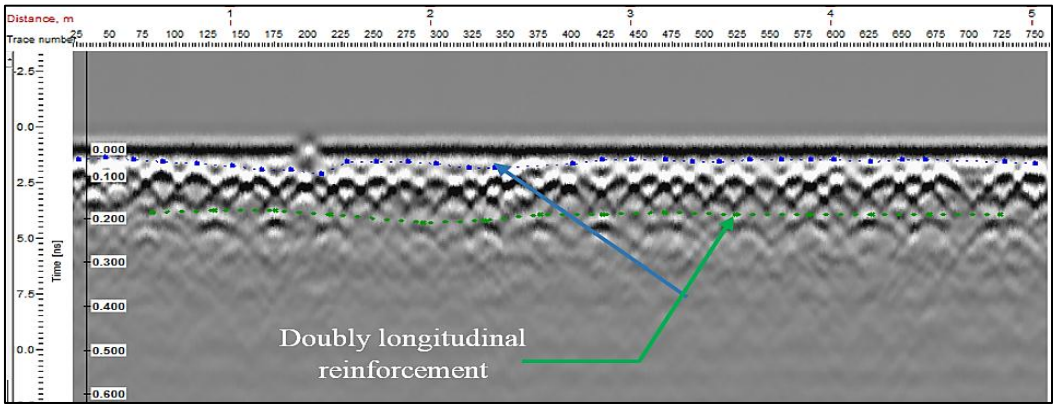

Figure 13: A radargram for Profile No. 29 showing the double longitudinal reinforcement.

Conclusions

From the intensive implementation of the GPR technique for pavement engineering investigations, the following conclusions are achieved:

1. Regarding evaluation best testing operation setting and processing of GPR, applying short, and 0.01 m point interval for 800 MHz is necessary to be employed for pavement investigation engineering.
2. For different structural pavements including the overlaid asphaltic layers and the composite structure, the outcomes suggests that the short 800 MHz frequency with 0.01 m point interval is clearly sufficient to distinguish the pavements layers thicknesses.

3. Comparisons between actual core thicknesses and that obtained by GPR equipment reveal the following outcomes:

   For overlaid flexible pavement: HMA overlay: 2 % error and ± 0.13 cm deviation.
   Surface layer: 2.5 % error and ± 0.2 cm deviation.
   Binder layer: approximately 0.6 % error and ± 0.61 cm deviation.

   For composite pavement

   Overlay: 4.5 % error and ± 0.2 cm deviation.
   Concrete layer: 2 % error and ±0.4 cm deviation.

4. For bridge inspection, the 2-D imaging radargrams gained by using 1 GHz offer massive date collection on a bridge deck that can be used to distinguish concrete damaged areas or corroded and deflected reinforcement. While 3-D imaging radargrams reflect better displays for the deteriorated or unclear signal of 2-D sections.
5. The amplitude through picking method can be very useful in determining the concrete cover or different materialistic layering. This conforms to pick accurate coordinates within short time period for long radar profiles and statistically plotted with reasonable accuracy.
6. The reflection picking method with assistance of the migration technique was found to be useful for integrated objects, continuous layered interface and uniform voltage amplitude textures.

References

Al-Qadi, I.L, Lahouar, S., Jiang, K., McGhee, K., and Mokarem, D., (2005), Validation of Ground Penetration Radar Accuracy for Estimating Pavement Layer Thicknesses, Paper No. 05-2341, Proceedings, Transportation Research Board 84th Annual Meeting, Washington, DC, pp. 9-13.

Amer, R., Saad, A., Elhafeez, T.A., Kady, H.E. and Madi, M., (2004), Geophysical and Geotechnical Investigation of Pavement Structures and Bridge Foundations, Austin J Earth Sci. Vol. 1, 6 P.

Barnes, C.L., Trottier, J.F., (2004), Effectiveness of Ground Penetrating Radar in Predicting Deck Repair Quantities, ASCE Journal of Infrastructure System, Vol. 10, pp. 69-76.

Bhandarkar, V.A., (1993), Detection of Sub-Surface Anomalies in Concrete Bridge Decks Using Ground Penetrating Radar, M.Sc thesis, Dept. of Civil Engineering, West Virginia University.

Charlton, M.B., (2008), Principles of ground-penetrating radar for soil moisture assessment, MBCharlton.com.

Conyers, L.B. and Goodman, D., (1997) Ground Penetrating Radar, An Introduction for Archaeologists, London: Altamira Press.

Davis, J.L. and Annan, A.P., (1989), Ground-penetrating radar for high-resolution mapping of soil and rock stratigraphy, Geophysical Prospecting, Vol. 37, pp.531-551.

Griffin, S., and Pippett, T., (2002), Ground Penetrating Radar, Geophysical and Remote Sensing Methods for Regolith Exploration, report 144, pp. 80-89.

Moore, J.R., Echard J.D., and Neill C.G., (1980), Radar Detection of Voids under Concrete Highways, Institute of Electrical and Electronics Engineers, New York, Paper 6-80-0131.

Muller, W., (2001), Ground Penetrating Radar (GPR) - Its applications within Main Roads and results of recent Concrete and Timber Field Trials, Presented at Road System and Engineering Technology Forum, Road System and Engineering Group, Queensland Department of Main Roads.

Reynolds, J. M., (1997), An Introduction to Applied and Environmental Geophysics, West Sussex, John Wiley & Sons Ltd, 796 P.